Solid-State NMR Investigation of the Structural Consequences of Plastic Deformation in Polycarbonate. 1. Global Orientational Order

Marcel Utz,† Ayman S. Atallah, Pierre Robyr, Albert H. Widmann, Richard R. Ernst, and Ulrich W. Suter*

Department of Materials, Institute of Polymers, and Department of Chemistry, Physical Chemistry, ETH, CH-8092 Zürich, Switzerland

Received January 19, 1999; Revised Manuscript Received June 9, 1999

ABSTRACT: The global orientational order that develops in polycarbonate under plastic deformation has been measured quantitatively by CSA and dipolar DECODER experiments. The results are in substantial agreement with the predictions of an affine entanglement network model. Athermal atomistic simulations, on the other hand, tend to overestimate the orientational order. The orientation behavior in glassy polycarbonate seems to be essentially the same as that in the melt.

1. Introduction

The plastic deformation of glassy polymers, like that of other amorphous solids, continues to present a challenge to materials science.[1] The behavior of such materials under plastic deformation constitutes a technologically and scientifically important aspect of their mechanical properties.[2] In spite of considerable research efforts, the elementary processes of deformation in polymer glasses have not yet been identified. As a consequence, no relationships have been established that would permit the prediction of plastic properties from the molecular structure of polymers. The work presented in this paper aims at contributing toward this goal by quantitatively investigating the structural consequences of plastic deformation.

On a macroscopic scale, the stress−strain behavior of glassy polymers has been studied extensively, and reliable constitutive models have been put forward.[3−7] Considerable effort has also been devoted to the caloric effects associated with plastic deformation.[8,9] These studies have shown that up to a deformation of about 40% most of the mechanical work done on the material is stored as internal energy. Beyond that point, the work of deformation is increasingly dissipated as heat.[9] This finding opens the interesting question which degrees of freedom actually absorb this increase in internal energy. Plastic deformation of glassy polymers is in general recoverable; i.e., a deformed sample reverts to its original shape if heated after the deformation. Interestingly, shape recovery sets in slightly above the deformation temperature, not only at the polymer's glass transition.[9]

Many authors have studied the orientational anisotropy in deformed polymers using optical techniques, such as polarized IR and Raman spectroscopy or birefringence.[10,11] However, most studies have focused on samples deformed in the melt state, i.e., above their glass-transition temperature.

Our strategy to identify the atomistic mechanism of plastic deformation in glassy polymers is to monitor the structural changes, on an atomistic length scale, that are induced by the deformation. The structural characterization of glassy solids is a difficult problem in general.[12] Experimental methods that could rival the specificity and resolution of diffraction techniques for crystalline solids have not been available for materials devoid of long-range translational order. Multidimensional solid-state NMR spectroscopy,[13−15] in view of its considerable progress over the past few years,[16] has the greatest potential to fill this methodological gap. It is particularly well suited to study orientational order, exploiting the orientational dependence of the interactions in the spin Hamiltonian.

The orientation of a molecular segment can be specified with respect to an external, macroscopic frame of reference or with respect to a microscopic one, for instance, an adjacent molecular segment. A deviation from uniformity of the distribution of molecular orientations is referred to as global or local orientational order, depending on whether a macroscopic or a microscopic frame of reference is chosen.

The global orientational order as a result of plastic deformation in polycarbonate has been studied previously[17] by Vogt et al. using the two-dimensional (2D) magic-angle-spinning NMR technique.[18] However, the tensile mode of deformation used in that study leads to mechanical instability and a correspondingly inhomogeneous deformation. This complicates the interpretation of the results in terms of a particular mechanism of plastic deformation. Also, subtle changes in the ring flip dynamics have been observed in deformed polycarbonate by 2D deuterium exchange spectroscopy by Hansen et al.[19,20] These authors have used a dedicated NMR probe assembly that allowed measurements in situ while the sample was loaded. Again, a tensile mode of deformation was used, which limited the accessible strain to only a few percent.

Compressive modes of deformation are preferable, since mechanical instabilities can be avoided more easily than in tension. Utz et al. have quantified the orientational order in a polycarbonate sample compressed uniaxially to a strain of $\epsilon = -0.4$,[21] measuring one-dimensional (1D) spectra of specifically ^{13}C-labeled samples at different angles of the deformation axis and the static magnetic field. This work demonstrated the feasibility of quantifying changes in the orientational

† Present address: Department of Chemical Engineering, Princeton University, Princeton NJ 08540.

10.1021/ma9900611 CCC: $18.00
Published on Web 09/01/1999

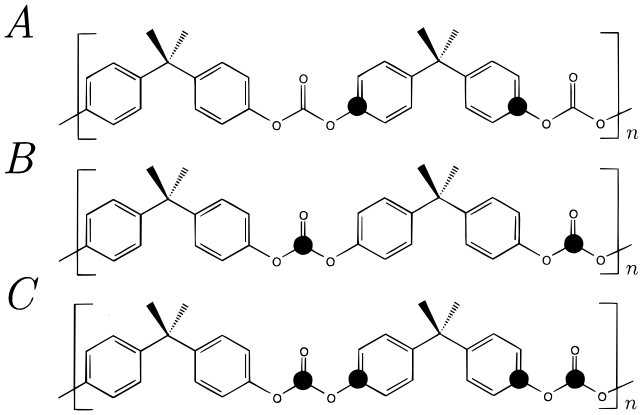

Figure 1. Repeat units of bisphenol A polycarbonate samples, enriched to 99% with ^{13}C at the positions indicated by the heavy dots. (A) aromatic label (al-PC). (B) carbonate label (cl-PC). (C) double label (dl-PC).

order of polycarbonate induced by large deformations below the glass-transition temperature.

In the present contribution, we report results from a more extended study, using plane-strain compression in a channel-die apparatus as mode of deformation. The global orientational order at different degrees of deformation was quantified by measuring the orientational distribution functions of three different molecular frames of reference using the chemical shielding anisotropy (CSA)[22−24] and dipolar[25] variants of the DECODER technique. The data thus obtained are compared to athermal atomistic simulations as well as to the predictions of a simple model based on the concepts of rubber elasticity.

A companion paper[26] will report results on local orientational order which have been obtained from the same samples using double quantum and spin diffusion techniques.

2. Materials and Methods

^{13}C-Labeled Polycarbonate. The NMR methods applied in this contribution rely on bisphenol A poly(carbonate) (PC) samples specifically enriched with ^{13}C at the carbonate, the oxygen-bound phenylene, or at both sites. In the following, we will briefly discuss the terms governing the spin dynamics in these systems.

The molecular segment under study is shown in Figure 1

A−C. Three different types of ^{13}C-labeled polycarbonate have been synthesized in the course of earlier work.[27] They are enriched to 99% of ^{13}C at the oxygen-bound aromatic site in every second bisphenol A unit (al-PC, Figure 1A), at the carbonate site (cl-PC, Figure 1B), or both (dl-PC, Figure 1C). In the case of dl-PC, 20% of labeled material was dissolved in 80% of polycarbonate with natural isotopic abundance (na-PC) in order to isolate the two-spin systems from one another.

As determined from static 1D powder spectra at 135 K,[27] the chemical shielding tensor at the carbonate unit (C1, see Figure 2) exhibits an anisotropy of $\delta = 87$ ppm and an asymmetry of $\eta = 0.39$. For the phenylene unit (C2), the corresponding values are $\delta = 94$ ppm and $\eta = 0.55$. (For a definition of the parameters δ and η, see Schmidt-Rohr and Spiess[16]). At ambient temperature, molecular motion leads to partial averaging of the chemical shielding anisotropy (CSA). Apparent CSA parameters at 300 K are $\delta = 89$ ppm and $\eta = 0.39$ for the carbonate and $\delta = 92$ ppm and $\eta = 0.54$ for the

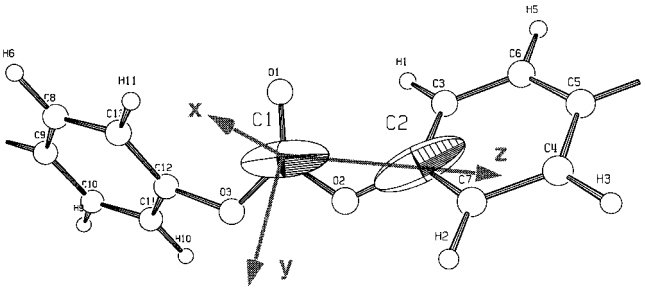

Figure 2. Ball-and-stick representation of a section of the polycarbonate chain. The ellipsoids around C1 and C2 represent the chemical shielding tensors at the carbonate and the phenylene label, respectively. The axes of the molecular frame of reference (MF) are shown.

phenylene site. (The room temperature values have been determined from static 1D spectra in the course of this study. They do not correspond exactly to those indicated in Tomaselli et al.,[27] which contains printing errors. On the basis of the accepted value for the isotropic shift of the carbonate site,[28] the above values for δ and η correspond to CSA eigenvalues of $\sigma_{xx} = 84.9$ ppm, $\sigma_{yy} = 120.1$ ppm, and $\sigma_{zz} = 236.4$ ppm for the carbonate site and $\sigma_{xx} = 77.9$ ppm, $\sigma_{yy} = 127.2$ ppm, and $\sigma_{zz} = 239.9$ ppm for the phenylene site.)

The alignment of the principal axis systems (PAS) of the chemical shift tensors with the molecular structure can be inferred to about 5° accuracy by comparison with analogous low-molecular-weight compounds.[27] For the carbonate unit (C1), the *y*-axis (intermediate shielded) is perpendicular to the C1−O1−O2 plane, whereas the *x*-axis (most shielded) is aligned with the C1−O1 double bond (Figure 2). This is the inverse of what has been assumed previously,[21,27−29] and corresponds to the revised orientation of the carbonate chemical shielding tensor published recently by Robyr et al.[30]

At the phenylene site (C2), the *z*-axis (least shielded) is aligned with the O2−C2 bond, while the *x*-axis coincides with the normal to the phenylene ring plane (Figure 2).

Reference Frames. We introduce the following reference frames and rotations between them:

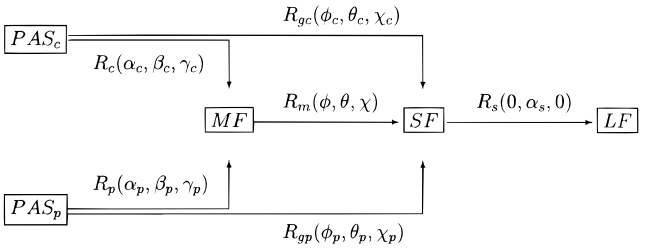

Here, PAS_c and PAS_p denote the principal axis systems of the carbonyl and the phenylene chemical shielding tensor, respectively. MF is the molecular axis system, the *z*-axis of which coincides with the vector between the atoms C1 and C2 and the *x*-axis of which is given by the normal of the (C1−O2−C2) plane (cf. Figure 2). With this choice, the unique axis of the dipolar interaction tensor between C1 and C2 is the *z*-axis of the molecular axis system. SF is the sample axis system, and LF denotes the laboratory frame of reference. The probe assembly that has been used in this work (cf. Experimental Section) allows rotation of the sample about an axis perpendicular to the magnetic field. This axis of rotation is chosen as the *y*-axis of LF,

with z_{LF} being the direction of the magnetic field. α_s is the sample rotation angle. R_p and R_c are the rotation operators that rotate PAS_p and PAS_c into MF.

The bond lengths and bond angles in the repeat unit of polycarbonate can be inferred from X-ray studies on crystalline low-molecular-weight analogues of polycarbonate.[31] The rotation operators $R_{gc} = R_c R_m$ and $R_{gp} = R_p R_m$ rotate PAS_p and PAS_c into the sample frame. It is R_{gc}, R_{gp}, and R_m that are the subject of the present study.

The rotating frame Hamiltonian governing the evolution of an isolated (C1,C2) spin system under proton decoupling, relevant to the dl-PC sample, is given by

$$H = \Omega_1 S_{1z} + \Omega_2 S_{2z} + b_{12}\left\{2S_{1z}S_{2z} - \frac{1}{2}(S_1^+ S_2^- + S_1^- S_2^+)\right\} \quad (1)$$

where Ω_1 and Ω_2 are the rotating frame precession angular frequencies of the two spins and b_{12} is the dipolar coupling between them. In the case of the cl-PC and al-PC samples, only the first or the second term remains, respectively.

With the Cartesian rotation matrices $\boldsymbol{R}_c$, $\boldsymbol{R}_p$, $\boldsymbol{R}_m$, and $\boldsymbol{R}_s$ corresponding to the rotations R_c, R_p, R_m, and R_s, respectively, the angular frequencies and the dipolar coupling can be expressed as

$$\Omega_1 = -\gamma B_0 \left(\boldsymbol{R}_s^T \boldsymbol{R}_m^T \boldsymbol{R}_c^T \begin{bmatrix} \delta_x^c & 0 & 0 \\ 0 & \delta_y^c & 0 \\ 0 & 0 & \delta_z^c \end{bmatrix} \boldsymbol{R}_c \boldsymbol{R}_m \boldsymbol{R}_s \right) \quad (2)$$

Ω_2 analogously with R_c being replaced by R_p and δ_i^c by δ_i^p, and

$$b_{12} = \frac{d}{2}\left(\boldsymbol{R}_s^T \boldsymbol{R}_m^T \begin{bmatrix} 1 & 0 & 0 \\ 0 & 1 & 0 \\ 0 & 0 & -2 \end{bmatrix} \boldsymbol{R}_m \boldsymbol{R}_s \right)_{33} \quad (3)$$

with the coupling constant

$$d = \frac{\mu_0}{4\pi} \frac{\gamma_s^2 \hbar}{r_{12}^3} \quad (4)$$

where $r_{12} = |\overrightarrow{C1,C2}|$. The 33 subscript denotes the 33 elements of the resultant matrix.

DECODER Measurements. A one-dimensional NMR experiment delivers for each interaction tensor just a single observable frequency, insufficient to determine the full orientation or its distribution function. Sometimes it is possible to take advantage of several tensor interactions, rigidly related to the same molecular fragment, where more orientational information is available, although its evaluation (e.g., in the case of an angular distribution) might be ambiguous. A somewhat related problem lies in the fact that the NMR experiment is axially symmetric around the direction of the static magnetic field. Without further precautions, only the uniaxial average of the orientational distribution function can be derived from NMR spectra, irrespective of the pulse sequence.

Several methods to overcome this limitation have been reported. In the simplest case, spectra can be recorded at several different orientations of the sample. Information on the orientational distribution function can then be obtained from a joint analysis of the data.[21]

More elegantly, Henrichs[22] proposed a two- or three-dimensional experiment where between the detection and the different evolution periods the sample is rapidly reoriented.[32] This breaks the uniaxial symmetry of the NMR experiment and allows for the correlated measurement of two or three frequencies associated with each interaction tensor, from which a unique orientation of the tensor and its full distribution function can be determined. Later, Schmidt−Rohr et al. coined the acronym DECODER for this experiment.[23,24,33] It has been applied to chemical shielding tensor,[23,24] quadrupolar tensor,[23] and dipolar tensor[25] measurements. In the following, we report results from CSA DECODER measurements on deformed al-PC and cl-PC and from dipolar DECODER measurements on dl-PC samples.

Data Analysis. An orientational distribution function is a normalized, positive function of three Euler angles $P(\phi,\theta,\chi)$. The orientation of a molecular segment is described by the rotation $R(\phi,\theta,\chi)$ from the reference frame into the molecular frame. The latter is often chosen to coincide with the principal axis frame of the interaction tensor that is used for the experimental characterization of the orientational distribution function. As P is normalized, it is square-integrable. Hence, it is possible to decompose it into a series of Wigner matrix elements[34,35]

$$P(\phi,\theta,\chi) = \sum_{j,m,m'} c^j_{mm'} D^j_{mm'}(\phi,\theta,\chi) \quad (5)$$

where either integer or half-integer j can be used.[36] In the following, we will always assume integer j. The coefficients $c^j_{mm'}$ are given as

$$c^j_{mm'} = \frac{2j+1}{8\pi^2} \int_0^{2\pi} d\phi \int_0^{\pi} d\theta \sin\theta \times \int_0^{2\pi} d\chi\, P(\phi,\theta,\chi)\, D^{j*}_{mm'}(\phi,\theta,\chi)$$
$$= (2j+1)\langle D^j_{mm'}(\phi,\theta,\chi)\rangle \quad (6)$$

where the asterisk denotes the complex conjugate. The quantities $\langle D^j_{mm'}(\phi,\theta,\chi)\rangle$ are known as moments of the orientational distribution function or as "order parameters". Due to orthorhombic (D_{2h}) symmetry on the level of the sample (which can be assumed here due to the experimental setup) and on the level of the molecular segments (which is given by the symmetry of the terms in the secular spin Hamiltonian), only Wigner matrix elements with positive, even indices j,m,m' need to be taken into account.

Orientational distribution functions (ODF) can be determined from the DECODER spectra using the conjugate orthogonal functions (COF) approach.[12] This scheme yields two sets of orthogonal functions, one in the domain of ODF (eigenfunctions), and one in the spectral domain (eigenspectra). Experimental data is then interpreted simply by projection onto the eigenspectra. The COF calculations have been carried out in a symmetry-adapted basis set constructed from Wigner matrix elements,[37] such that order parameters $\langle D^j_{mm'}\rangle$ could easily be obtained from the experimental data. Computer programs for the calculation of the COF eigenfunctions and eigenspectra of DECODER experiments have been written in FORTRAN and were run

on a Sun Ultra-2 workstation. A typical run using a Wigner matrix basis up to $j = 20$, corresponding to 506 different basis functions, and spherical integration on a grid of 4×10^4 points took about 2 min of CPU time.

Sometimes, it is desirable to indicate the orientational distribution function of a molecular director, i.e., a direction fixed in the molecular frame of reference, specified by two polar angles (Θ, Φ). The orientational distribution function of the molecular z-axis is given by integration over the third Euler angle:

$$\bar{P}(\alpha,\beta) = \int_0^{2\pi} P(\alpha,\beta,\gamma)\mathrm{d}\gamma = 2\pi \sum_{j,m} c^j_{m0} D^j_{m0} \tag{7}$$

The distribution function of any molecular direction (Θ, Φ) can therefore easily be found by applying a rotation that orients the (Θ, Φ)-axis parallel to the z-axis of the reference frame before the rotation $R(\alpha\beta\gamma)$. This results in a transformed orientational distribution function $\tilde{P}(\alpha\beta\gamma)$, which can be integrated over the third Euler angle in order to obtain the desired directional distribution function $P_{\Theta,\Phi}(\alpha,\beta)$. Using the addition theorem for the Wigner matrix elements[36] and the abbreviation $R^j_{kn} = D^j_{kn}(0, -\Theta, -\Phi)$ we obtain

$$\begin{aligned}\tilde{P}(\alpha\beta\gamma) &= \sum_{jmn} c^j_{mn} \sum_k D^j_{mk}(\alpha\beta\gamma) R^j_{kn} \\ &= \sum_{jmnk} c^j_{mn} R^j_{kn} D^j_{mk}(\alpha\beta\gamma) \\ &= \sum_{jmk} \underbrace{\left(\sum_n c^j_{mn} R^j_{kn}\right)}_{\tilde{c}^j_{mk}} D^j_{mk}(\alpha\beta\gamma)\end{aligned} \tag{8}$$

From this, we find by integration over γ

$$P_{\Theta,\Phi}(\alpha,\beta) = 2\pi \sum_{j,m} D^j_{m0} c^j_{m0}(\alpha\beta 0) \tag{9}$$

Hence, the problem of finding the orientational distribution of a general vector in the molecular frame amounts to a simple unitary transformation of the expansion coefficients $c^j_{mm'}$.

3. Experimental Section

Nuclear Magnetic Resonance. NMR measurements were conducted on a home-built spectrometer operating at a proton resonance frequency of 220 MHz.[29] The radio frequency (rf) field strength was adjusted to 50 kHz for Hartmann−Hahn cross polarization and for I-spin decoupling and to 100 kHz for short rf pulses. The Hartmann−Hahn contact time was 2 ms in all cases. A time of 80 ms was necessary for the completion of a 90° flip in the DECODER experiments. Nevertheless, the flip delay was set to 200 ms to allow for the decay of any mechanical vibrations the sample flip might have caused. It was demonstrated by recording two−dimensional spectra at a flip angle of 180° that the spin−diffusion contribution is negligible for the DECODER experiments.

Sample Preparation. The synthesis of the three types of specifically ^{13}C-labeled polycarbonate samples (Figure 1) used in this study has been described in detail elsewhere.[27] The molecular weights and the polydispersities of the isotopically enriched material are given in Table 1.

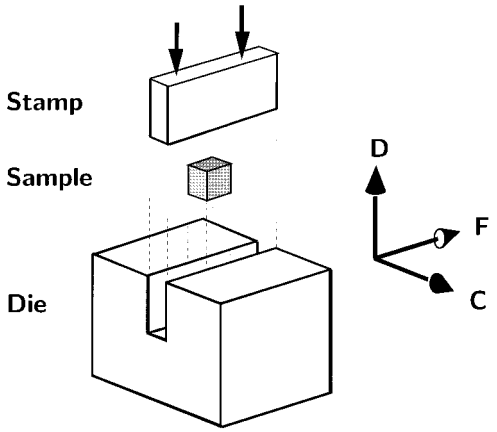

Figure 3. Schematic drawing of the channel-die extrusion experiment. The sample (center) fits into the channel of the die. The sample is extruded in the channel by means of a stamp. The entire setup is fitted to a mechanical testing machine. The experiment produces plane strain and is characterized by the three distinct directions F (free), C (constraint), and D (deformation).

Table 1. Molecular Weight and Polydispersity of the Polycarbonate Samples

sample	M_w	M_w/M_n
al-PC	31 700	1.4
cl-PC	30 500	1.5
dl-PC	36 200	1.5
na-PC	30 500	1.5

For the deformation experiments, dense, rectangular samples were needed, adapted in shape to the dimensions of the channel die. This was accomplished by first dissolving the polymer in dichloromethane to give a 2 wt % solution. In the case of the dl-PC, 20 wt % of the labeled material and 80% of natural abundance polycarbonate were dissolved together. The polymer was then precipitated by slowly casting the solution into the 10-fold volume of agitated, dry, cold methanol. After suction filtration, the material was dried at 60 °C under vacuum (<10 mbar) for 24 h. Samples of 5 mm height, 5 mm width, and 10 mm length were obtained by compression of the material in a rectangular die by means of a heated-plate ram. The die was surrounded by a copper mantle to enhance heat transfer from the plates of the press. A load of 2 GPa was applied at 250 °C during 2 min. After that, the die was removed from the copper heating mantle and slowly (>40 min) cooled to room temperature under a load of less than 0.1 GPa. Inspection of the dense samples under polarized light showed no trace of inhomogeneity.

Plastic Deformation. The plane-strain deformation was executed in a home-built channel-die setup (Figure 3) at 300 K. The channel die was fitted to a mechanical testing machine (Zwick, Germany) that was programmed such that the remaining separation between the die and the stamp followed an exponential decay, leading to a constant strain rate $\dot{\epsilon} = -0.001\ \mathrm{s}^{-1}$. Together with the relatively slow strain rate, the large thermal mass of the channel die ensured isothermal conditions. To combine good resistance to corrosion with favorable heat-conduction properties, a ferritic stainless steel (X20Cr13) was used for the construction of the

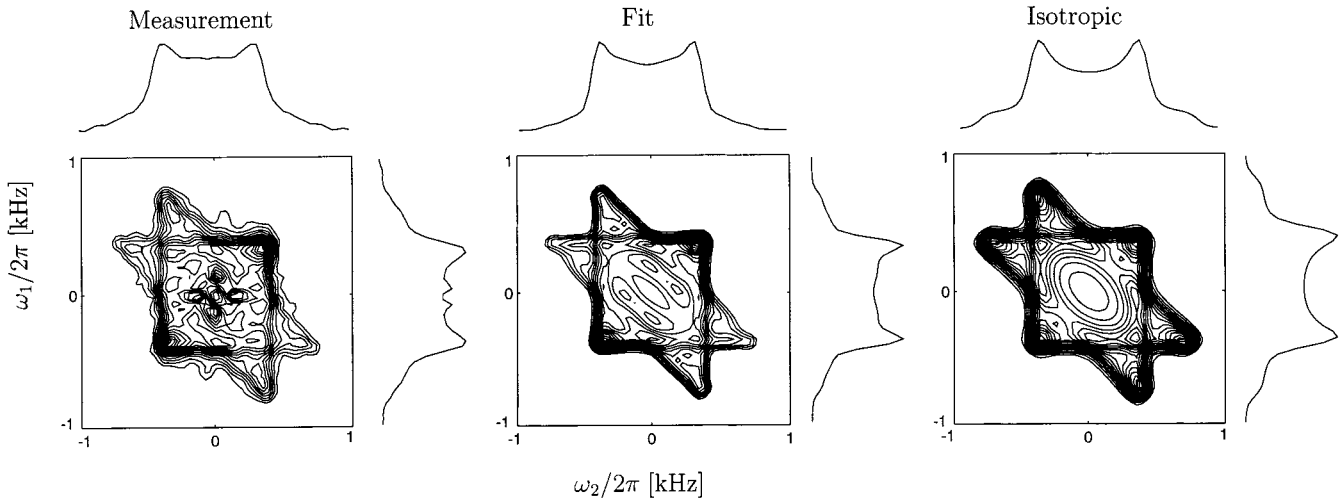

Figure 4. Dipolar DECODER spectrum of a sample deformed under plane strain to $\epsilon = -0.68$. Left: experimental spectrum. Center: fit using 30 COF eigenfunctions. Right: spectrum calculated for a perfectly isotropic sample. The artifact visible in the center of the measured spectrum stems from spurious natural abundance ^{13}C nuclei, the response of which has imperfectly been suppressed at the data processing stage.

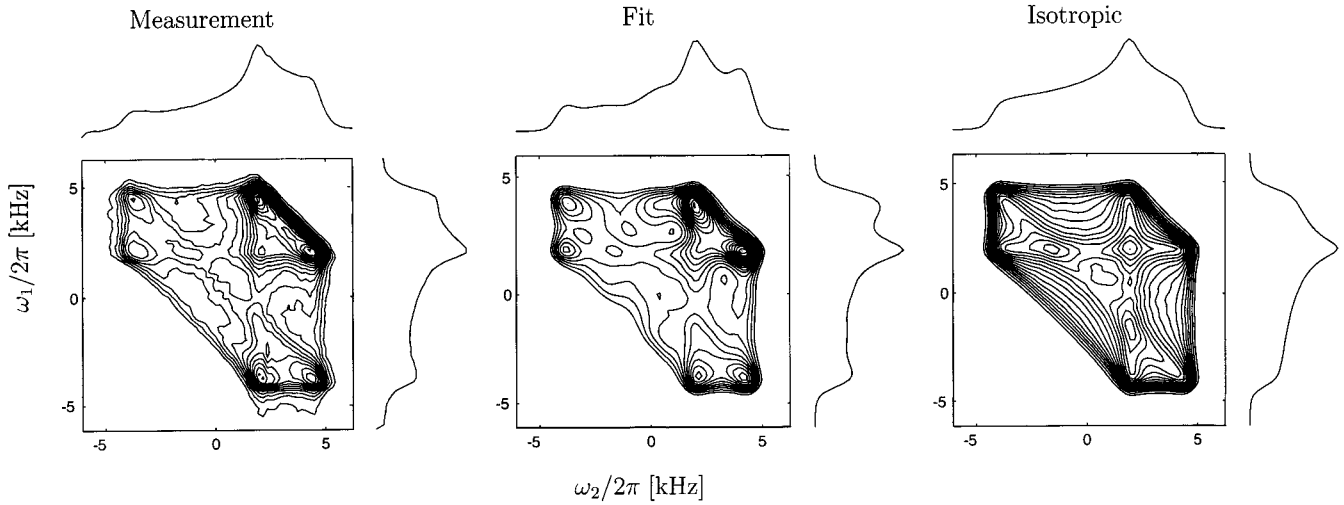

Figure 5. CSA DECODER spectrum of a polycarbonate sample labeled with ^{13}C at the phenylene ring (al-PC), at a plane strain deformation of $\epsilon = -0.61$. Left: measurement. Center: fit using 30 COF eigenfunction. Right: calculated isotropic spectrum.

channel die. To ensure the full slip boundary condition between the die and the polymeric glass, the sample was wrapped in teflon ribbon and a perfluorinated lubricant was used. The strain data from the deformation experiments were corrected for the finite compliance of the testing machine, which was measured independently by running an experiment with the channel die empty.

4. NMR Results

Dipolar and CSA DECODER spectra have been recorded from two different deformed samples of each type of labeling. In each case, one of the two samples was deformed to a plane strain of $\epsilon \approx -0.4$ and one to $\epsilon \approx -0.6$. A dipolar and a CSA DECODER spectrum are shown in Figures 4 and 5, respectively, along with their COF fits. The resulting orientational distribution functions are given in terms of their first few order parameters in Table 2.

In the case of the chemical shielding tensors, which are truly three-dimensional objects, a full orientational distribution function of three Euler angles results. The dipolar interaction, due to its axial symmetry, only yields a distribution function of two polar angles; therefore, only order parameters with the second lower index equal to 0 are indicated in Table 2.

Table 2. Order Parameters Determined from Dipolar and CSA DECODER Spectra[a]

	dl-PC		al-PC		cl-PC	
ϵ=	−0.44	−0.68	−0.36	−0.61	−0.42	−0.55
$\langle D^2_{00}\rangle$	−55 ± 04	−67 ± 04	−66 ± 19	−77 ± 19	−79 ± 03	−91 ± 03
$\langle D^2_{02}\rangle$			02 ± 04	03 ± 04	−15 ± 03	−17 ± 03
$\langle D^2_{20}\rangle$	−28 ± 33	−33 ± 31	−19 ± 16	−47 ± 16	−26 ± 07	−57 ± 07
$\langle D^2_{22}\rangle$			−07 ± 24	−09 ± 24	12 ± 13	07 ± 13
$\langle D^4_{00}\rangle$	−65 ± 16	−65 ± 15	51 ± 03	52 ± 03	45 ± 21	37 ± 21
$\langle D^4_{02}\rangle$			−16 ± 02	−16 ± 02	00 ± 06	01 ± 06
$\langle D^4_{04}\rangle$			03 ± 11	04 ± 11	−08 ± 06	−08 ± 06
$\langle D^4_{20}\rangle$	10 ± 04	07 ± 03	08 ± 01	12 ± 01	17 ± 00	16 ± 00
$\langle D^4_{22}\rangle$			−02 ± 06	01 ± 06	−05 ± 06	−04 ± 06
$\langle D^4_{24}\rangle$			04 ± 02	04 ± 02	−01 ± 00	−01 ± 00
$\langle D^4_{40}\rangle$	−05 ± 09	01 ± 08	51 ± 02	52 ± 02	56 ± 03	55 ± 03
$\langle D^4_{42}\rangle$			09 ± 02	09 ± 02	06 ± 04	06 ± 04
$\langle D^4_{44}\rangle$			−08 ± 08	−07 ± 08	03 ± 01	03 ± 01

[a] All values are to be multiplied by 10^{-3}. The indicated errors are standard deviations.

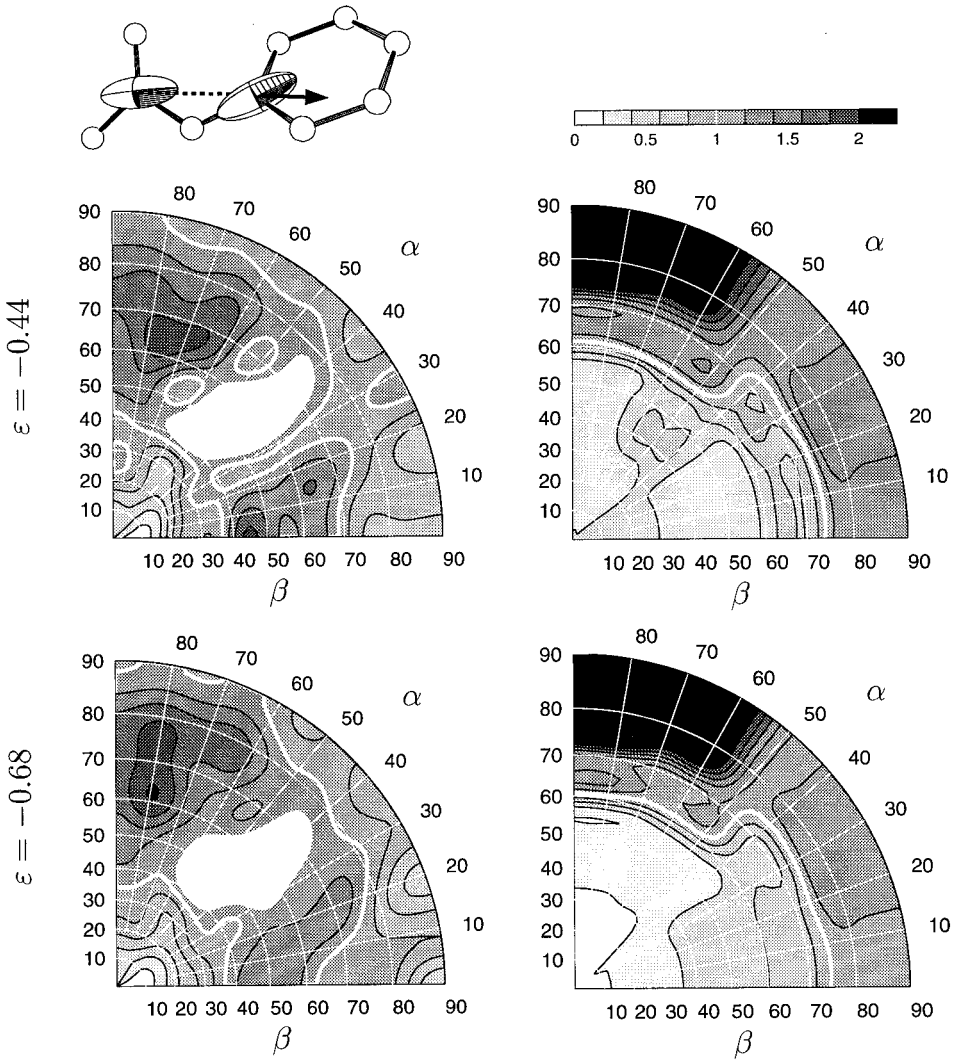

Figure 6. Polar diagrams of the *z*-axis of the molecular frame of reference (vector connecting C1 and C2). Upper row: $\epsilon = -0.44$. Lower: $\epsilon = -0.68$. Left: experimental data. Right: athermal atomistic simulations.

Orientational distribution functions are difficult objects to visualize, in particular in the fully three-dimensional case. The directional distribution functions corresponding to the principal axes of the interaction tensors are shown as polar diagrams in Figures 6−12, along with the corresponding data obtained from athermal simulations. These plots use a stereographic projection as it is used in pole figures and display a uniform level of 1 for a random spatial distribution of a vector. The origin in each polar diagram corresponds to alignment of the respective molecular direction with the deformation (*D*) axis of the channel die, whereas the lower right ($\beta = 90°$, $\alpha = 0$) and the upper left ($\beta = 90°$, $\alpha = 90°$) corners correspond to the constrained (*C*) and free (*F*) directions, respectively.

The molecular axis system for all three molecular segments under study has been chosen such that the local *z*-axis points roughly along the polymer chain. As is evident from Table 2, $\langle D^2_{00} \rangle$ provides the dominant contribution to the anisotropy in all cases,[38] reflecting the preferential orientation of the chain vector parallel to the free direction of the channel die. The same basic trend is also visible in the polar diagrams: the strongest deviations from uniformity occur in Figures 6, 9, and 12.

The polar diagrams derived from the dipolar DECODER spectra (Figure 6) contain an artifact at $\alpha = 45°$ and $\beta = 54.7°$. This is due to the presence of natural abundance ^{13}C nuclei in the samples, which give rise to a strong peak at $\omega_1 = \omega_2 = 0$ in the dipolar DECODER spectra.[25] Imperfect suppression of this peak (cf. Figure 4) leads to a corresponding "blind spot" artifact in the polar diagrams.

5. Modeling

Several authors have put forward ad hoc kinematic mechanisms for the elementary process of plastic deformation in glassy polymers.[1,39,40] Most of these mechanisms have in common that they focus on conformational changes in the polymer chains, leading to highly localized processes (on the order of 10 atoms) that produce locally a large increment of shear (on the order of 100%).

The model proposed by Robertson[39] postulates two possible local conformations of the polymer chains: an energetically favored, translike (extended) and an energetically disfavored, cislike (flexed) conformation. Robertson assumes that under shear stress the population of flexed segments is transiently increased, leading to an increase in the "structural temperature" of the solid. Robertson estimates the strain-induced increase in structural temperature from the geometry of the cis−trans isomerization and from the energy difference

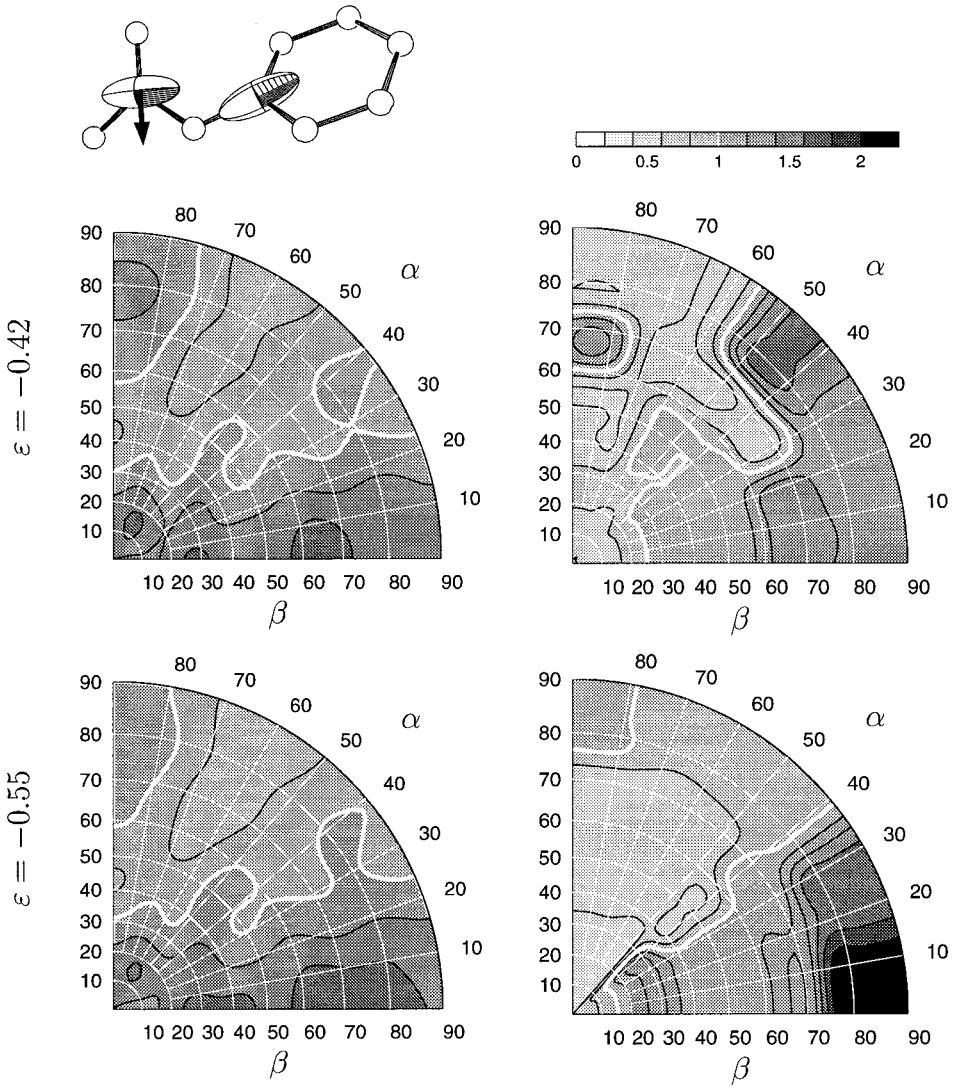

Figure 7. Polar diagrams of the *x*-axis in the carbonate group. Top row: $\epsilon = -0.42$. Bottom: $\epsilon = -0.55$. Left: measurement. Right: athermal simulation.

between the two states and then uses the Willams−Landel−Ferry equation[41] to estimate the viscosity. Robertson's theory is impressively successful in predicting the yield stress of glassy polymers close to their glass-transition temperature, but it predicts an arbitrarily high yield stress at low temperature, which is not observed in practice. Yannas and Luise[40] make the conformational change and its intramolecular energetics the central point of their model.

Whereas the mechanism of Robertson is purely concerned with intramolecular effects, Argon[42] has proposed a model based on the gradual alignment of polymer chains by the motion of kinks in the molecular conformation. Argon estimates the change in free energy associated with the formation of a pair of kinks from the elastic strain that they induce into their surroundings, thus focusing on intermolecular aspects of the deformation process. His model predicts a stress dependence of the activation energy of the plastic flow process. Therefore, there is a limiting stress at which the material flows even at absolute zero, leading to a better description of the low-temperature behavior of polymer glasses.

None of the hitherto proposed heuristic models of polymer deformation make any explicit prediction on the global orientational order that develops as a function of deformation.

Athermal atomistic simulations, based on gradual deformation of the simulation box under repeated energy minimization with respect to the torsional degrees of freedom in the polymer chain have been carried out on polypropylene[43−45] and on polycarbonate.[46] In both cases, none of the deformation kinematics previously proposed in heuristic models could be identified. Rather, the plastic relaxation events extended throughout the entire simulation box, suggesting that the elementary processes of plastic deformation in polymers are highly cooperative, involving volumes well beyond the largest simulation boxes (10 nm^3).

Mott et al. have observed a slight deviation from spherical symmetry in the ODF of the "bond-chord" vectors in PP.[45] They indicated this result in terms of the asphericity *a*, which is a measure of the deviation from spherical symmetry that can be shown to be a quadratic form of the moments $\langle D^2_{00}\rangle$ and $\langle D^2_{20}\rangle$. At a pure shear deformation of $\epsilon \approx -0.2$, Mott et al. observed an increase in asphericity of $\Delta a = 0.008$. A corresponding analysis has not been reported for polycarbonate.

5.1. Affine Entanglement Network (AEN) Model. As a model for the segment orientation under deforma-

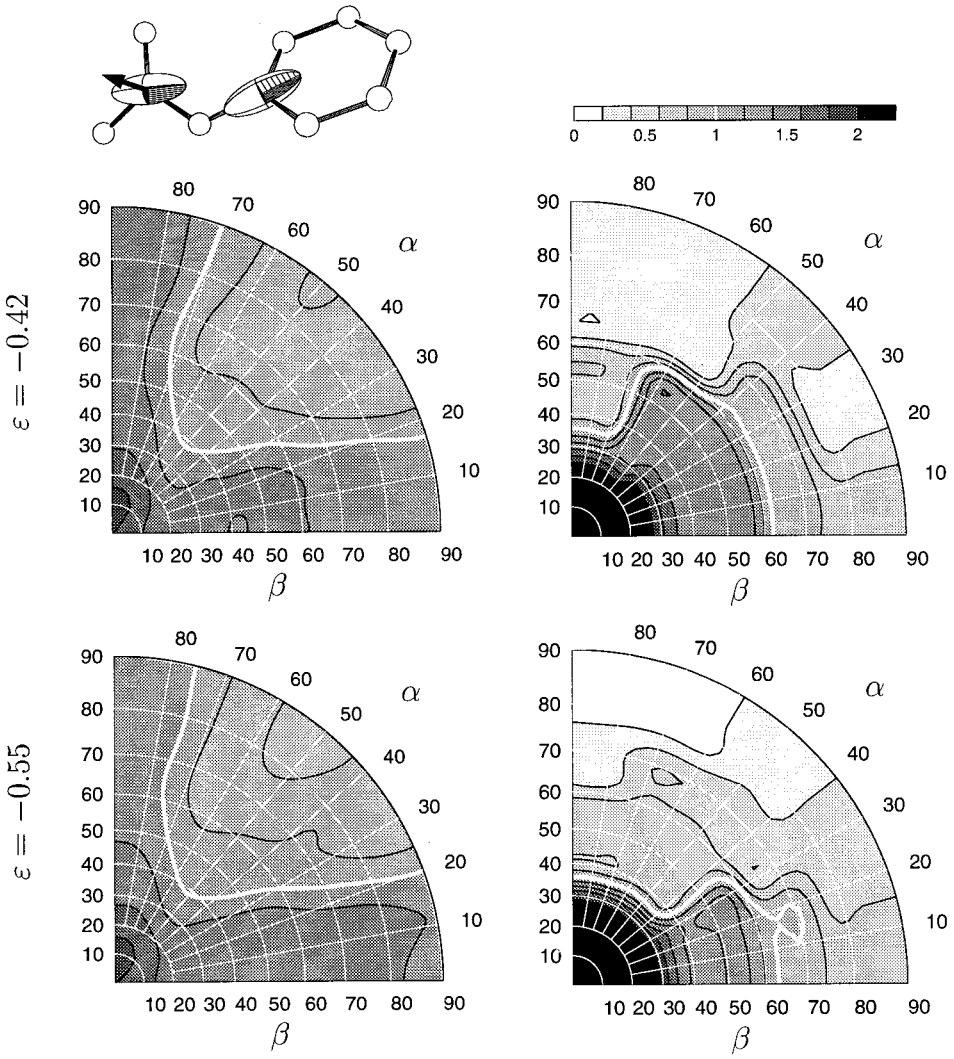

Figure 8. Polar diagrams of the *y*-axis in the carbonate group. Top row: $\epsilon = -0.42$. Bottom: $\epsilon = -0.55$. Left: measurement. Right: athermal simulation.

tion, the polymer was tentatively assumed to behave like a rubber with a cross-link density corresponding to the entanglement[47] density of polycarbonate. Whereas the application of rubber elasticity for the modeling of the strain hardening response is questionable (due to the intrinsic assumption of ergodicity, although it leads to quite reliable constitutive models for glassy polymers[3,4,7,48]), similar concerns do not arise for the description of segmental orientation, as the configurational entropy is not used in this case. Universal sampling of the configuration space is not assumed for each individual chain; only the average of the orientational distribution of the chain segments over all chains is taken to correspond to thermal equilibrium, which is a much weaker assumption.

The most likely orientational distribution function of the molecular segments of a polymer chain around the end-to-end vector can then be described by the expression derived by Kuhn and Grün.[49] The transformation of vectors between material points follows the macroscopic kinematics of the deformation, if the two material points are far enough apart. For atomically proximate material points, the kinematics is obviously quite different, since bond lengths and bond angles cannot be expected to change noticeably. The main assumption of the AEN model lies in the fact that the *crossover between microscopic and macroscopic kinematics is at the length scale of the entanglement network*. The only parameter of the model is the number of statistical segments between the entanglement points.

The most likely orientational distribution function of the chain elements in a freely jointed chain has been derived by Kuhn and Grün:[49,50]

$$P(\beta) = \frac{b}{2 \sinh b} \exp(b \cos \beta) \quad b = L^{-1}\left(\frac{r}{nl}\right) \quad (10)$$

where β is the angle between the end-to-end vector and the chain segment, r is the length of the end-to-end vector, n is the number of statistical segments, and l is their length. $L^{-1}(x)$ denotes the inverse Langevin function. The orientational distribution function resulting from the deformation of a rubber network can be calculated from eq 10 by assuming an initially isotropic ensemble of chains, each with an initial end-to-end distance $r_0 = l(n)^{1/2}$. With the chain extension ratio $\lambda_c = r/r_0$, b becomes

$$b = L^{-1}(\lambda_c/\sqrt{n}) \quad (11)$$

and the orientational distribution function $P(\beta)$ only depends on the ratio $\lambda_c/(n)^{1/2}$. Using the first nontrivial term of the Taylor expansion of eq 10, Kuhn and Grün have calculated $\langle D_{00}^2 \rangle$ for uniaxial extension as a func-

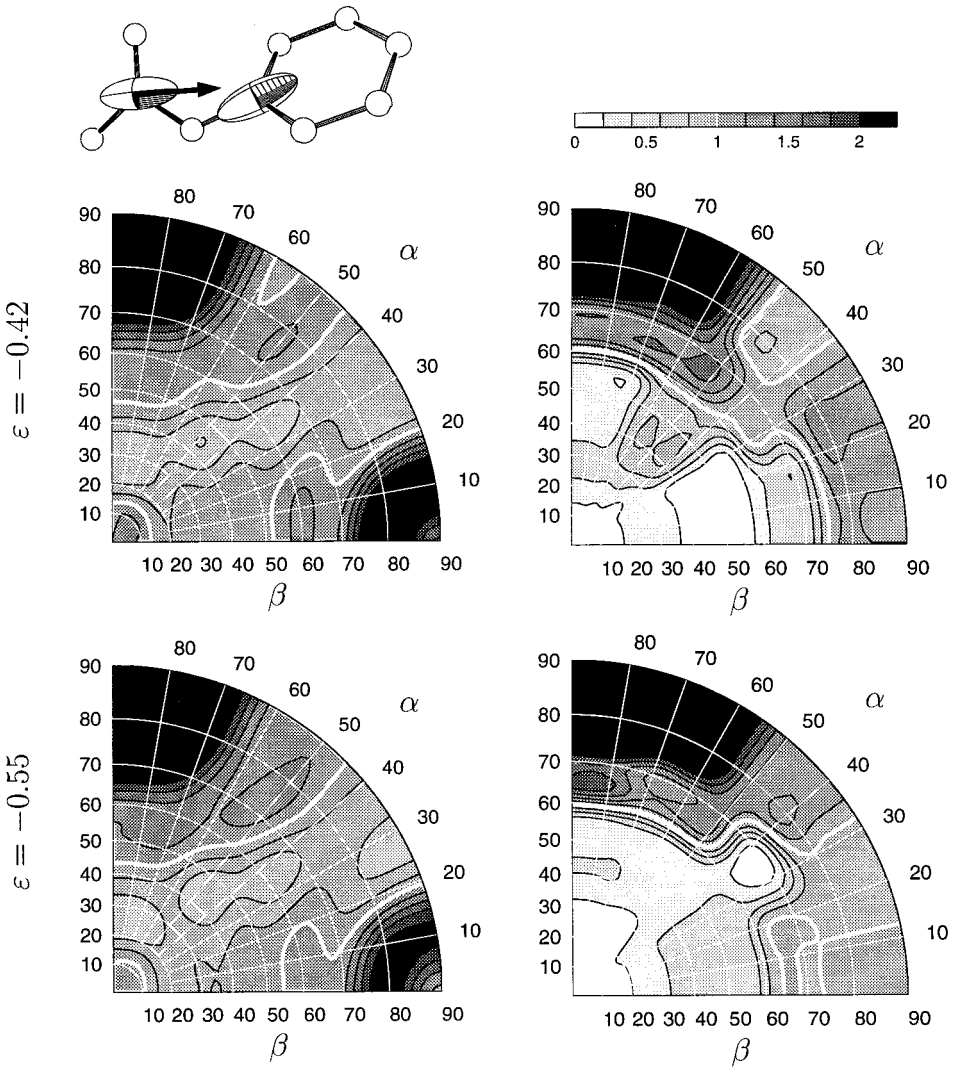

Figure 9. Polar diagrams of the *z*-axis in the carbonate group. Top row: $\epsilon = -0.42$. Bottom: $\epsilon = -0.55$. Left: measurement. Right: athermal simulation.

tion of the extension ratio λ to be[49]

$$\langle D^2_{00} \rangle = \frac{1}{5n}\left(\lambda^2 - \frac{1}{\lambda}\right) \tag{12}$$

Here, we are interested in plane-strain deformation, rather than uniaxial extension. Moreover, the Taylor approximation used by Kuhn and Grün is only valid for small extension ratios compared to $(n)^{1/2}$. For an AEN of polycarbonate, $(n)^{1/2}$ has a value of about 2. The highest deformation that has been studied corresponds to a linear extension ratio of $\lambda = 2$, which is obviously not a small number by comparison.

For a single chain, the orientational distribution function $P(\beta)$ can be described by the order parameters

$$M^j_{00}(\lambda_c/\sqrt{n}) = \int_0^\pi P(\beta)\, D^j_{00}(0\beta 0) \sin\beta \, \mathrm{d}\beta \tag{13}$$

Using the first Padé approximant for the inverse Langevin function,

$$L^{-1}(x) \approx \frac{x(3 - x^2)}{1 - x^2} \tag{14}$$

which is a very good approximation,[7,51] these moments can be calculated analytically, although the expressions become rather complicated.

The end-to-end vector of a deformed chain, normalized by its original length and oriented at polar angles (θ, ϕ) *in the deformed sample* is given by

$$\frac{\mathbf{r}}{|\mathbf{r}_0|} = \lambda_c \begin{bmatrix} \cos\phi \sin\theta \\ \sin\phi \sin\theta \\ \cos\theta \end{bmatrix} = \begin{bmatrix} \lambda_x \cos\phi' \sin\theta' \\ \lambda_y \sin\phi' \sin\theta' \\ \lambda_z \cos\theta' \end{bmatrix} \tag{15}$$

where $\lambda_{x,y,z}$ are the linear extension ratios given by the Cauchy−Green tensor and (θ',ϕ') are the polar angles of the end-to-end vector *before* deformation. The quantities $\theta = \theta(\theta', \phi'; \lambda_{x,y,z})$, $\phi = \phi(\theta', \phi'; \lambda_{x,y,z})$, and $\lambda_c = \lambda_c(\theta', \phi'; \lambda_{x,y,z})$ can easily be calculated by solving the system of equations (15). Using the rotational transformation laws of the Wigner matrix elements, the order parameters of the orientational distribution of the molecular segments can be calculated from the single-chain order parameters M^j_{00} as

$$\langle D^j_{\mathrm{m}0} \rangle (\lambda_x,\lambda_y,\lambda_z) = \frac{1}{2\pi}\int_0^\pi \int_0^{2\pi} M^j_{00}\left(\frac{\lambda_c}{\sqrt{n}}\right) D^j_{\mathrm{m}0}(\phi,\theta,0) \sin\theta' \, \mathrm{d}\phi' \, \mathrm{d}\theta' \tag{16}$$

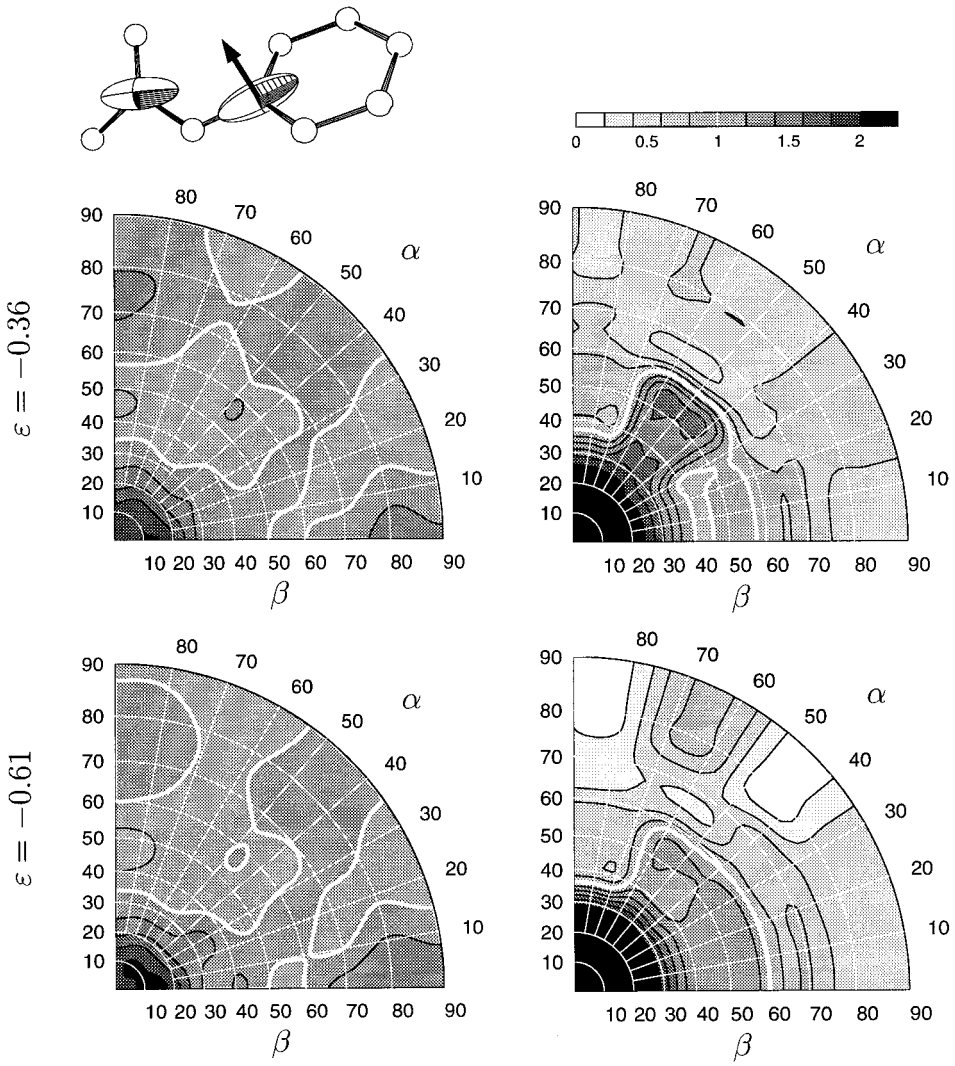

Figure 10. Polar diagrams of the *x*-axis in the phenylene group. Top row: $\epsilon = -0.36$. Bottom: $\epsilon = -0.61$. Left: measurement. Right: athermal simulation.

This integral is impractical to evaluate analytically; therefore, it must be approximated by a suitable quadrature rule. In the simplest case, this is accomplished by using the eight-chain model by Arruda and Boyce.[52] More precise results, particularly for higher values of *j*, are obtained by using the spherical Gaussian quadrature rule proposed by Edén and Levitt.[53] Indeed, the eight-chain model yields nonzero values for the moments with $j \geq 4$ even in the undeformed state, whereas Gaussian spherical quadrature guarantees vanishing moments up to $j = 24$, using only 10 sampling points in the relevant octant of the unit sphere.

Figure 13 compares the values of $\langle D^2_{00} \rangle$ predicted for uniaxial extension by eq 16, the eight-chain model of Arruda and Boyce[3] and the approximation of Kuhn and Grün, eq 12. All three expressions agree quite well up to extensions of $\lambda = 1.5$, whereas for higher λ, both the eight-chain model and Kuhn and Grün's expression underestimate the orientational order.

5.2. Athermal Simulation. Atomistic simulations of the deformation of glassy polymers have been pioneered by Mott et al.[44−45] and Hutnik et al.[46] These authors have introduced the athermal simulation method, where the periodic cell containing the polymer model is deformed in small steps and the potential energy of the system is minimized with respect to the internal degrees of freedom of the atomistic model after each deformation step.

Here, similar simulations have been carried out on polycarbonate, with the goal of predicting the global orientational order as a function of plane-strain deformation. These simulations differ slightly from those reported by Hutnik et al. A substantially larger simulation cell was used (60 nm^3 instead of 8 nm^3). Moreover, the molecular model used here was flexible, based on Cartesian coordinates, and allowed for small readjustments of bond lengths and bond angles, whereas in the simulations by Hutnik et al., only torsional angles were mobile. To allow for the comparison to experimental results, a plane-strain mode of deformation was used, which is equivalent, up to a unitary rotation, to the pure shear mode that was employed by Hutnik et al.

Amorphous structures of seven individual chains with 25 monomer units each were generated by the packing algorithm proposed by Müller et al.[54,55] This algorithm packs the chains according to a target conformation, minimizing the overlaps of nonbonded atoms using a hard-sphere potential. To switch to a more realistic potential, the energy of the packed structure was minimized using the pcff91 force field,[56] and then, the structure was thermalized under the same force field for 50 ps at 300 K. The thermalized structures were

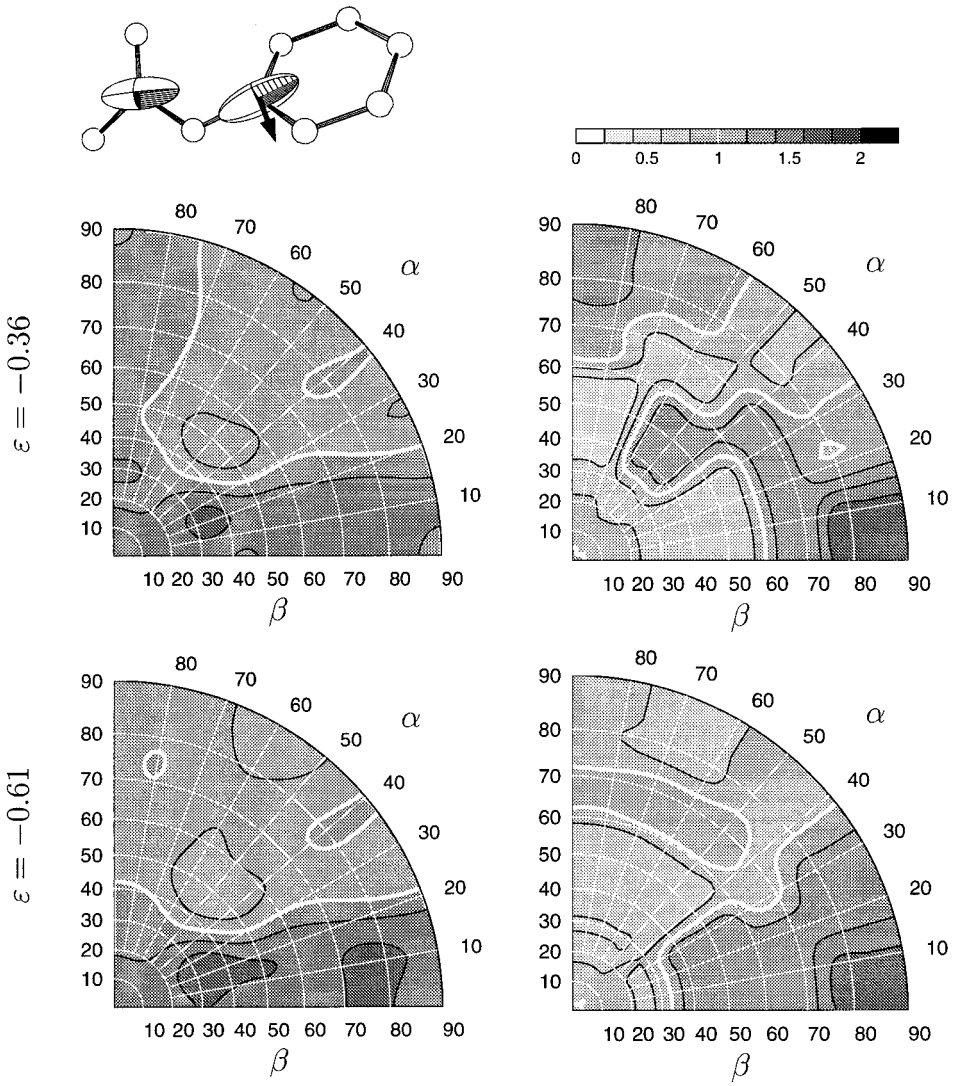

Figure 11. Polar diagrams of the *y*-axis in the phenylene group. Top row: $\epsilon = -0.36$. Bottom: $\epsilon = -0.61$. Left: measurement. Right: athermal simulation.

submitted to the athermal plane-strain protocol.

Figure 14A shows the typical[43−46] saw-tooth response of the potential energy in an athermal simulation. As the cell is deformed, the potential energy increases until a saddle point on the energy landscape of the system is reached. The following structural relaxation, which has been shown[43−46] to extend throughout the simulation cell, releases most of the potential energy, leading to a very gradual net increase. Above $\epsilon = -0.7$, the energy starts to increase more steeply, indicating that the resistance of the model to plastic deformation becomes substantially stronger beyond this point.

The distribution of strain increments $\Delta\epsilon$ between two successive relaxation events is shown in Figure 14B. A log-normal distribution function has been fitted to the data. The corresponding partial distribution function (dashed line in Figure 14B) has its maximum around $\Delta\epsilon = 0.02$. This finding is in good agreement with the transition shear strain increment $\Delta\gamma^T$ of about 2% that was found for both polypropylene[44] and polycarbonate.[46]

The simulation has been carried out in steps of $\delta\epsilon = -0.005$. After each deformation increment and minimization, the atomic coordinates were stored. Subsequently, Euler angles and Wigner moments were obtained from this information. Directional distribution functions have been calculated as histograms, dissecting the relevant octant of the unit sphere in 6×6 patches of an equal spherical angle. For plotting, the resulting histograms have been interpolated using a cubic spline algorithm, increasing the number of sampling points by a factor of 9. Polar diagrams showing the directional distribution functions resulting from simulation are shown, along with the corresponding experimental data, in Figures 6−12.

The order parameters resulting from the athermal simulation for the phenylene and for the carbonate site are represented in Figure 15 by light gray bars. Data for the two degrees of deformation realized experimentally are shown, along with the corresponding experimental data (black; cf. Table 2) and the predictions of the affine entanglement network model (gray) where applicable. For the latter, the number of statistical segments between entanglement points n has been estimated from the conformational properties of polycarbonate with

$$n = \frac{M_e l_0^2}{m_0^2}\left(\frac{\langle r^2\rangle_0}{M}\right)^{-1} \tag{17}$$

where m_0/l_0 is the linear specific mass and $\langle r^2\rangle_0/M$ is the mass-specific mean-square end-to-end distance. Taking

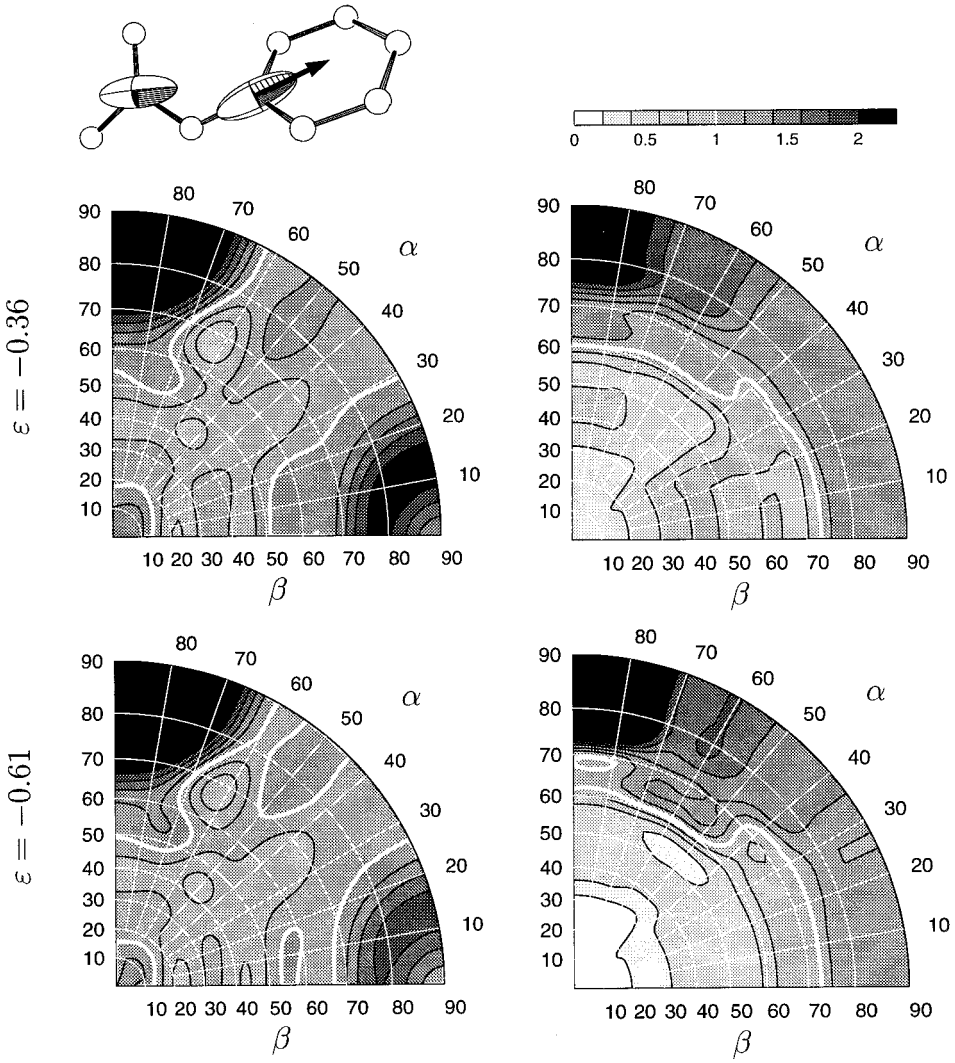

Figure 12. Polar diagrams of the *z*-axis in the phenylene group. Top row: $\epsilon = -0.36$. Bottom: $\epsilon = -0.61$. Left: measurement. Right: athermal simulation.

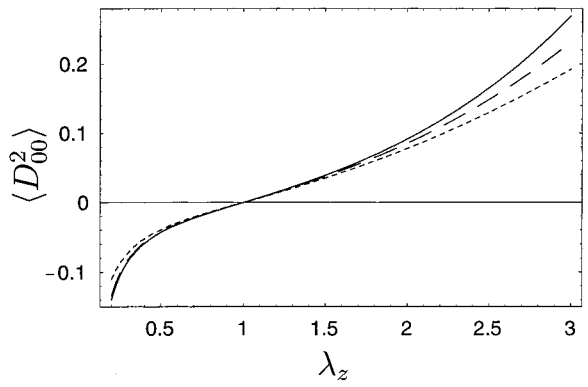

Figure 13. Comparison of the exact expression, eq 16 (solid line), with the eight-chain model by Arruda and Boyce[52] (dashed line) and Kuhn and Grün's approximation, eq 12 (dotted line), for $\langle D^2_{00} \rangle$ as a function of uniaxial extension at constant volume. In all cases, $n = 9$.

experimental data,[57] a value of $n \approx 4$ results.

6. Discussion

It is quite obvious from Figure 15 and from the polar diagrams that the anisotropies predicted by the athermal simulations are substantially larger than what is observed experimentally. However, it is noteworthy that *qualitatively*, the agreement is quite good. The simulations correctly predict enrichment of the vectors pointing along the polymer chain in the free direction (Figures 6, 9, and 12) and a preference for low angles α and β in the case of the carbonate and phenylene plane normals (Figures 8 and 10). In all cases, the signs of the order parameters predicted from athermal simulation agree with those of the measured data (Figure 15). It can therefore be concluded that while the athermal simulations substantially overestimate the magnitude of the orientation process, they seem to correctly capture its kinematics.

The AEN model, on the other hand, is in much better agreement with the experimental data. Because it describes the polymer as a chain of freely jointed segments of cylindrical symmetry, it cannot predict order parameters $\langle D^j_{mm'} \rangle$ with $m' \neq 0$. The order parameters $\langle D^2_{m0} \rangle$, however, agree astonishingly well with those obtained from measurement both at the phenylene and at the carbonate site, as well as the internuclear vector (Figure 15).

The observed orientation behavior is similar for all three frames of reference studied. As the *z*-axes of the three frames of reference are known to be predominantly aligned to within a small angle with the local chain direction in the undeformed state of the poly-

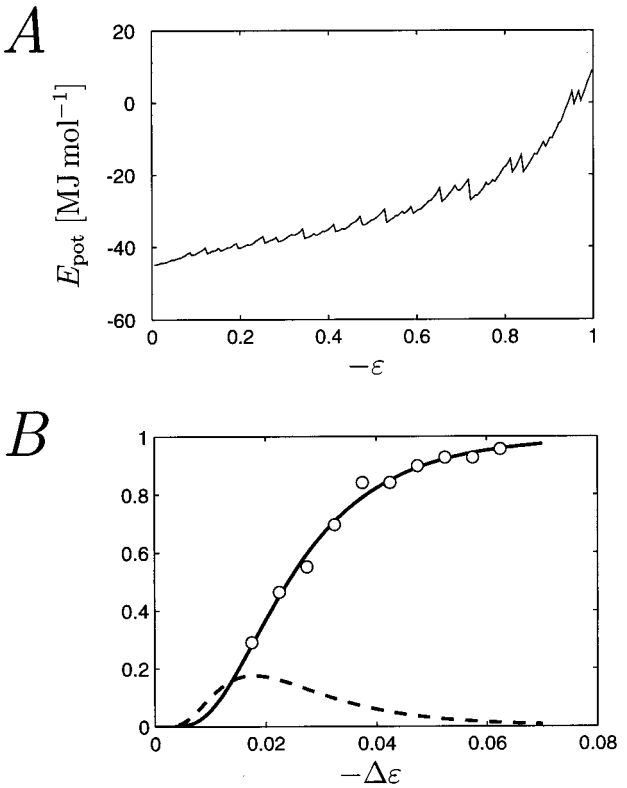

Figure 14. (A) Evolution of the potential energy of a 60 nm^3 simulation cell of PC under plane strain. The energy increases with deformation until a relaxation event occurs that dissipates most of it, generating a characteristic "saw-tooth" response. A pronounced increase in energy only occurs at strains larger than 0.6. (B) Distribution of deformation increments $\Delta\epsilon$ between plastic relaxation events. The solid and broken lines represent the cumulative and the partial distribution function, respectively.

mer,[12,27] this could be explained by the hypothesis that the molecular segment under study here essentially rotates as a rigid body under deformation. As shown in detail in the companion paper,[26] this hypothesis is corroborated by the finding that the distribution of dihedral angles between the labeled sites is unaffected by the deformation process.

The athermal simulations suffer from several limitations that must be considered as potential causes for their failure to predict the orientation behavior quantitatively. The most obvious limitation is the finite volume of the simulation cell of about 60 nm^3. The deformation is forced, by construction, to be affine at the level of the cell. By comparison to the AEN model, which assumes affine deformation at a length scale corresponding to the volume per entanglement (which is about 2 nm^3 for polycarbonate), this is a weak constraint. Therefore, it seems unlikely that the overestimation of the order parameters by the simulation is a finite size effect. Simulations with cells of different sizes, ranging from 10 nm^3 to 60 nm^3, showed no difference in the orientation behavior, as expected from the foregoing argument.

Another shortcoming of the simulations is also connected to the cell size: As is well-known,[1,44] atomistic simulations cannot model the localization of the plastic transitions. Doing so would require cell volumes 1 to 2 orders of magnitude above those affordable with presently available computer hardware. The elementary transitions in the simulations therefore extend throughout the simulation cell, rather than occurring in regions of finite size immersed in an elastic stress bath. The constraint of constant volume, which is immanent to the simulation protocol, may therefore influence the deformation process. A better simulation protocol which drives the deformation of the cell by coupling to an elastic stress bath, rather than by directly altering the cell parameters, is in development,[58] and studies regarding this problem are underway. Nevertheless, given the robustness of the order parameters with respect to the cell size mentioned above, it seems unlikely that this new procedure will lead to a sufficient reduction of the

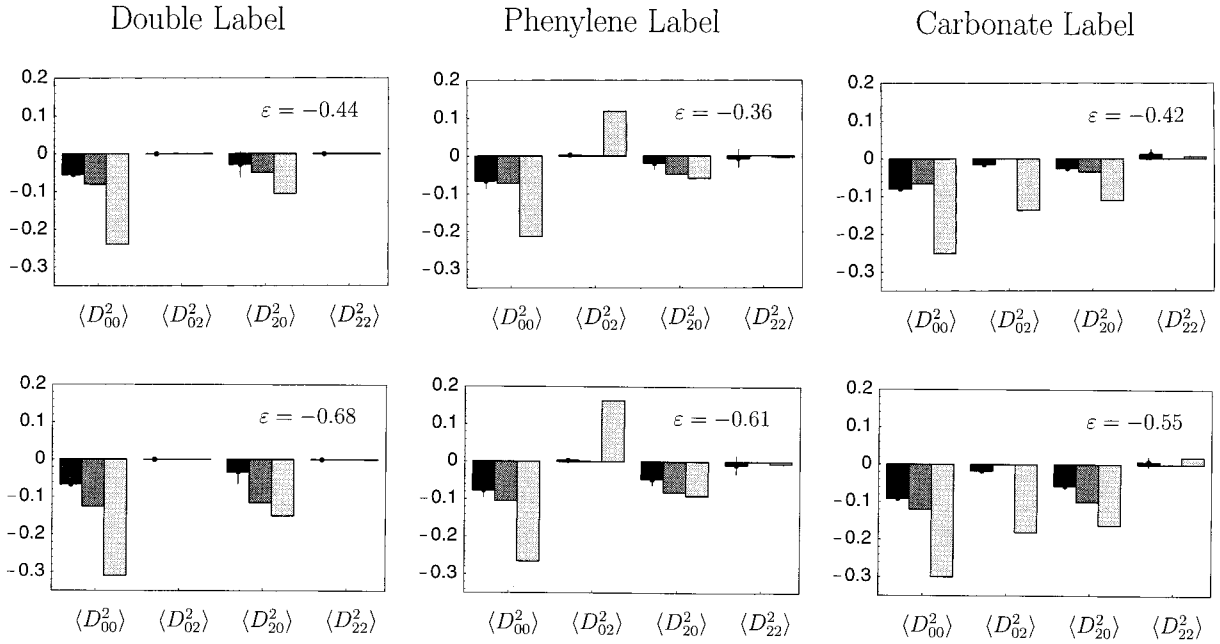

Figure 15. Comparison of order parameters obtained from the analysis of the DECODER data (black, with errors), the affine entanglement network model (gray), and athermal simulation (light gray). Left column: internuclear vector (dl-PC). Center column: phenylene site (al-PC). Right column: carbonate site (cl-PC). Data corresponding to two different degrees of deformation are shown (cf. Table 2), with $\epsilon \approx -0.4$ in the top row and $\epsilon \approx -0.6$ in the bottom.

estimated order parameters to bring them into agreement with the experimental data.

The most likely cause of the disagreement between experiment and simulation is the athermal nature of the latter. The AEN model is based on the assumption that the orientational distribution function of the chain segments between entanglement points corresponds to the most likely distribution at all times. The success of the AEN model in predicting the orientation behavior could be explained by the hypothesis that sufficient mobility exists in the glassy polymer at room temperature for the chain segments to reach thermal equilibrium *up to the entanglement length scale*. This interesting finding is in contrast to what is commonly believed to to be the dynamic nature of a deeply supercooled polymer glass. Further experimental studies of the orientation behavior at very low temperature, as well as simulation efforts at finite temperature, are necessary to clarify this point.

7. Conclusions

The global orientational order of three different molecular frames of reference in plastically deformed polycarbonate has been quantified by CSA and dipolar DECODER measurements. Athermal atomistic simulations have been carried out which agree qualitatively with the experimental observations but strongly overestimate the degree of orientational order. By contrast, the affine entanglement network model is in substantial agreement with the experimental data. The orientation behavior of glassy polycarbonate, some 130 K below its glass transition temperature, therefore seems to be remarkably similar to that of the same polymer above T_g, in the entangled melt regime.

This finding is in agreement with a study based on optical and transmission electron microscopy by Henkee and Kramer,[59] who have found the limiting strain in shear bands and craze fibrils in a variety of polymers to correlate strongly with the entanglement density.

The conclusion that the geometry of the entanglement network is the most important structural parameter for the plastic behavior of glassy polymers, first drawn by Henkee and Kramer, is therefore supported by the global orientation data presented in this contribution.

Acknowledgment. We gratefully acknowledge helpful discussions with Serge Santos, Dr. Zbigniew Stachursky, as well as valuable technical support by Paul Signer and Joe Eisenegger. We also thank Dr. Ralf Kaestle, EMPA Zürich, for help with the deformation experiments, Christoph Scheurer for providing a routine for computing Wigner matrix elements with arbitrary indices, and Prof. Beat H. Meier for providing access to the solid-state NMR facilities in his laboratory. This work has been funded by the Swiss National Science Foundation.

References and Notes

(1) Argon, A. S. In *Inelastic Deformation and Fracture of Glassy Solids*; Materials Science and Technology, Vol. 1 (Plastic Deformation and Fracture of Materials): VCH: Weinheim, Germany, 1993; pp 462−508.
(2) Ward, I. M. *Mechanical Properties of Solid Polymers*; Wiley−Interscience: London, 1971.
(3) Arruda, E. M.; Boyce, M. C. *Int. J. Plast.* **1993**, *9*, 697−720.
(4) Arruda, E. M.; Boyce, M. C.; Quintus-Bosz, H. *Int. J. Plast.* **1993**, *9*, 783−811.
(5) Boyce, M. C.; Arruda, E. M.; Jayachandran, R. *Polym. Eng. Sci.* **1994**, *34*, 716−725.
(6) Arruda, E. M.; Boyce, M. C.; Jayachandran, R. *Mech. Mater.* **1995**, *19*, 193−212.
(7) Tervoort, T. A. Constitutive Modelling of Polymer Glasses. Ph.D. Thesis, Technical University Eindhoven, 1996.
(8) Hasan, O. A.; Boyce, M. C. *Polymer* **1993**, *34*, 5085−5092.
(9) Oleinik, E. F.; Salamatina, O. B.; Rudnev, S. N.; Shenogin, S. V. *Polym. Sci. U.S.S.R.* **1993**, *35*, 1532−1558.
(10) Monnerie, L. In *Developments in Oriented Polymers*; Ward, I. M., Ed., Elsevier: New York, 1987; Vol. 2.
(11) Ward, I. M., Ed. *Structure and Properties of Oriented Polymers*, 2nd ed., Chapman & Hall: London, 1997.
(12) Utz, M. *J. Chem. Phys.* **1998**, *109*, 6110−6124.
(13) Abragam, A. *Principles of Nuclear Magnetism*; Clarendon Press: Oxford, 1961.
(14) Mehring, M. *High Resolution NMR Spectroscopy in Solids*; NMR, Basic Principles and Progress, Vol. 11; Springer: Berlin, 1976.
(15) Ernst, R. R.; Bodenhausen, G.; Wokaun, A. *Principles of Nuclear Magnetic Resonance in One and Two Dimensions*; Clarendon Press: Oxford, 1987.
(16) Schmidt-Rohr, K.; Spiess, H. W. *Multidimensional Solid-State NMR and Polymers*; Academic Press: San Diego, 1994.
(17) Vogt, V.-D.; Dettenmaier, M.; Spiess, H. W.; Pietralla, M. *Colloid Polym. Sci.* **1990**, *268*, 22−27.
(18) Harbison, G. S.; Vogt, V.-D.; Spiess, H. W. *J. Chem. Phys.* **1987**, *86*, 1206−1218.
(19) Hansen, M. T.; Blümich, B.; Boeffel, C.; Spiess, H.; Morbitzer, L.; Zembrod, A. *Macromolecules* **1992**, *25*, 5542−5544.
(20) Hansen, M. T.; Spiess, H. W. *Colloid Polym. Sci.* **1993**, *271*, 446−453.
(21) Utz, M.; Tomaselli, M.; Ernst, R. R.; Suter, U. W. *Macromolecules* **1996**, *29*, 2909−2915.
(22) Henrichs, P. M. *Macromolecules* **1987**, *20*, 2099−2112.
(23) Schmidt-Rohr, K.; Hehn, M.; Schaefer, D.; Spiess, H. W. *J. Chem. Phys.* **1992**, *97*, 2247−2262.
(24) Chmelka, B. F.; Schmidt-Rohr, K.; Spiess, H. W. *Macromolecules* **1993**, *26*, 2282−2296.
(25) Utz, M.; Eisenegger, J.; Suter, U. W.; Ernst, R. R. *J. Magn. Reson.* **1997**, *128*, 217−227.
(26) Utz, M.; Robyr, P.; Suter, U. W.; Ernst, R. R., in preparation.
(27) Tomaselli, M.; Robyr, P.; Meier, B.; Grob-Pisano, C.; Ernst, R. R.; Suter, U. W. *Mol. Phys.* **1996**, *89*, 1663−1694.
(28) Henrichs, P. M.; Linder, M.; Hewitt, M.; Massa, D.; Isaacson, H. V. *Macromolecules* **1984**, *17*, 2412−2416.
(29) Tomaselli, M. *Development and Application of Some NMR Experiments for Studying Disordered Solids*, Ph.D. Thesis, ETH Zürich, Diss. No. 11455, 1996.
(30) Robyr, P.; Utz, M.; Gan, Z.; Scheurer, C.; Tomaselli, M.; Suter, U. W.; Ernst, R. R. *Macromolecules* **1998**, *31*, 5818−5822.
(31) Perez, S.; Scaringe, R. P. *Macromolecules* **1987**, *20*, 68−77.
(32) Carter, C. M.; Alderman, D. W.; Grant, D. M. *J. Magn. Reson.* **1985**, *65*, 183−186.
(33) Lewis, R. H.; Long, H. W.; Schmidt-Rohr, K.; Spiess, H. W. *J. Magn. Reson.* **1995**, *A115*, 26−34.
(34) Brink, D.; Satchler, G. *Angular Momentum*, 3rd ed.; Clarendon Press: Oxford, 1993.
(35) McBrierty, V. J. *J. Chem. Phys.* **1974**, *61*, 872−882.
(36) Varshalovich, D. A.; Moskalev, A. N.; Kheronskii, V. K. *Quantum Theory of Angular Momentum*; World Scientific: Singapore, 1988.
(37) Utz, M. *Investigation of Plastically Deformed Glassy Polymers by Solid-State NMR*, Ph.D. Thesis, ETH Zürich, Diss. No. 12717, 1998.
(38) In the case of dl-PC, the value of $\langle D_{00}^4 \rangle$ is strongly affected by the presence of the unwanted central peak in the dipolar DECODER spectra.
(39) Robertson, R. E. *J. Chem. Phys.* **1966**, *44*, 3950−3956.
(40) Yannas, I. V.; Luise, R. R. In *The Strength and Stiffness of Polymers*; Zachariades, R. E., Porter, R. S., Eds., Dekker: New York, 1983.
(41) Ferry, J. D. *Viscoelastic Properties of Polymers*, 3rd ed.; Wiley: New York, 1980.
(42) Argon, A. S. *Philos. Mag.* **1973**, *28*, 839−865.
(43) Argon, A. S.; Mott, P. H.; Suter, U. W. *Phys. Status Solidi B* **1992**, *172*, 193−204.
(44) Mott, P. H.; Argon, A. S.; Suter, U. W. *Philos. Mag. A* **1993**, *67*, 931−978.
(45) Mott, P. H.; Argon, A. S.; Suter, U. W. *Philos. Mag. A* **1993**, *68*, 537−564.
(46) Hutnik, M.; Argon, A. S.; Suter, U. W. *Macromolecules* **1993**, *26*, 1097−1108.
(47) Graessley, W. W. *Adv. Polym. Sci.* **1974**, *16*, 1.

(48) Arruda, E. M. Characterization of the Strain Hardening Response of Amorphous Polymers, Ph.D. Thesis, Massachusetts Institute of Technology, 1992.
(49) Kuhn, W.; Grün, G. *Kolloid-Z.* **1942**, *101*, 248−271.
(50) Treloar, L. R. G. *The Physics of Rubber Elasticity*, 3rd ed.; Clarendon Press: Oxford, 1975.
(51) Cohen, A. *Rheol. Acta* **1991**, *30*, 270.
(52) Arruda, E. M.; Boyce, M. C. *J. Mech. Phys. Solids* **1993**, *41*, 389−412.
(53) Edén, M.; Levitt, M. H. *J. Magn. Reson.* **1998**, *132*, 220−239.
(54) Müller, M.; Nievergelt, J.; Santos, S.; Suter, U. W. **1999**, submitted for publication.
(55) Santos, S.; Suter, U. W.; Müller, M.; Nievergelt, J. **1999**, submitted for publication.
(56) Maple, J. R.; Hwang, M.-J.; Stockfisch, T. P.; Dinur, U.; Waldman, M.; Ewig, C. S.; Hagler, A. T. *J. Comput. Chem.* **1994**, *15*, 162−182.
(57) Fetters, L.; Lohse, D.; Richter, D.; Witten, T.; Zirkel, A. *Macromolecules* **1994**, *27*, 4639−4647.
(58) Santos, S.; Gusev, A. A.; Suter, U. W.; Yang, J. S.; Jo, W. H. **1998**, submitted for publication.
(59) Henkee, C. S.; Kramer, E. J. *J. Polym. Sci., Polym. Phys.* **1984**, *22*, 721−737.

MA990061L